Article

Cell Systems

IKZF1 Enhances Immune Infiltrate Recruitment in Solid Tumors and Susceptibility to Immunotherapy

Graphical Abstract

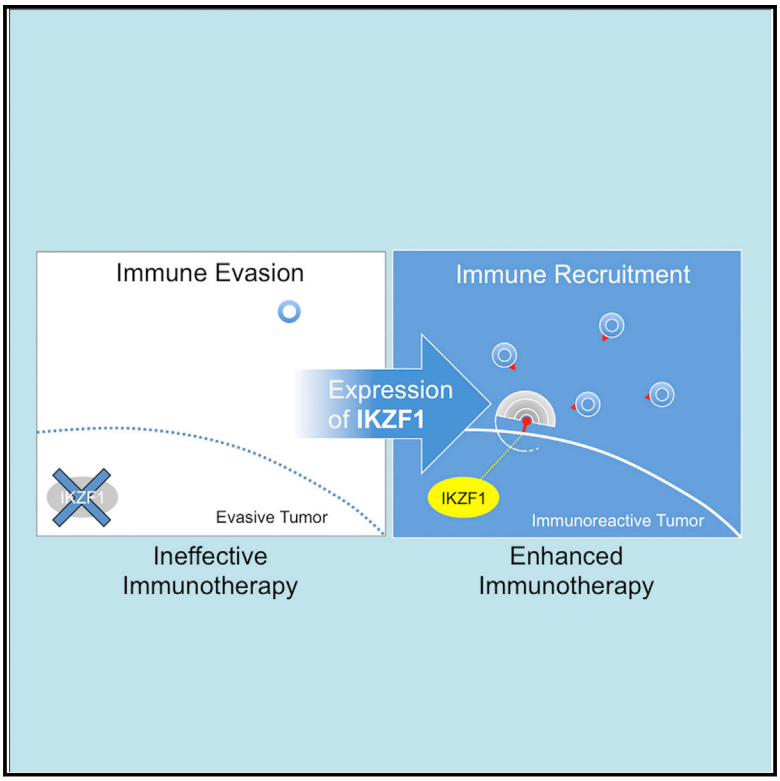

Highlights

- A network-based computational framework can identify key enhancers of immunotherapy
- IKZF1 overexpression promotes immune infiltrate recruitment in several tumor types
- IKZF1 overexpression in tumors enhances efficacy of α-PD1 and α-CTLA4 treatment
- Genomic alterations of IKZF1 predict poor prognosis and low immune infiltration

Authors

James C. Chen,
Rolando Perez-Lorenzo,
Yvonne M. Saenger, Charles G. Drake,
Angela M. Christiano

Correspondence

amc65@columbia.edu

In Brief

Immunotherapies are promising cancer treatments but are frequently stymied by tumors that evade the immune system. Here, Chen et al. computationally identify the regulators required to hijack and reactivate immune infiltrate recruitment in tumors. They show that IKZF1 expression suppresses growth in several cancers due to enhanced immune infiltrate recruitment and significantly enhances the efficacy of α-PD1 and α-CTLA4 immunotherapies. IKZF1 genomic alterations also predict poor prognosis in patient cohorts. This work demonstrates the value of computational approaches in identifying new treatment avenues.

Chen et al., 2018, Cell Systems 7, 92–103
July 25, 2018 Published by Elsevier Inc.
https://doi.org/10.1016/j.cels.2018.05.020

CellPress

CellPress

Cell Systems
Article

IKZF1 Enhances Immune Infiltrate Recruitment in Solid Tumors and Susceptibility to Immunotherapy

James C. Chen,[1,2] Rolando Perez-Lorenzo,[1] Yvonne M. Saenger,[4] Charles G. Drake,[4] and Angela M. Christiano[1,3,5,*]
[1]Department of Dermatology, Columbia University Medical Center, New York, NY, USA
[2]Department of Systems Biology, Columbia University Medical Center, New York, NY, USA
[3]Department of Genetics and Development, Columbia University Medical Center, New York, NY, USA
[4]Department of Medicine, Herbert Irving Comprehensive Cancer Center, Columbia University Medical Center, New York, NY, USA
[5]Lead Contact
*Correspondence: amc65@columbia.edu
https://doi.org/10.1016/j.cels.2018.05.020

SUMMARY

Immunotherapies are some of the most promising emergent treatments for several cancers, yet there remains a majority of patients who do not benefit from them due to immune-resistant tumors. One avenue for enhancing treatment for these patients is by converting these tumors to an immunoreactive state, thereby restoring treatment efficacy. By leveraging regulatory networks we previously characterized in autoimmunity, here we show that overexpression of the master regulator *IKZF1* leads to enhanced immune infiltrate recruitment and tumor sensitivity to PD1 and CTLA4 inhibitors in several tumors that normally lack *IKZF1* expression. This work provides proof of concept that tumors can be rendered susceptible by hijacking immune cell recruitment signals through molecular master regulators. On a broader scale, this work also demonstrates the feasibility of using computational approaches to drive the discovery of novel molecular mechanisms toward treatment.

INTRODUCTION

Immunotherapies are rapidly emerging as highly promising avenues of treatment across multiple cancer types, and additional research is consistently emerging that is dedicated to characterizing the complex interactions between the immune system and a growing tumor. However, studies have demonstrated that many patients do not benefit from treatments such as immune checkpoint inhibition (Topalian et al., 2015; Aggen and Drake, 2017; Emambux et al., 2018). Promoting and enhancing the efficacy of immunotherapies in additional patients and cancers, as well as the ability to predict and match patients to optimal treatments, would be invaluable scientific and medical advancements. One potential avenue for enhancement therapy is the conversion of immune-resistant tumors to an immunoreactive state by inducing immune sensitivity to cancers that have selectively acquired mechanisms to avoid immune surveillance.

The treatment paradigm of immune checkpoint inhibition specifically promotes host immune recognition of tumors, which can be countered at a molecular level by disabling the key pathways for such recognition and rendering these inhibitors ineffective (colloquially referred to as "immune evasion"). Overcoming these evasion mechanisms and restoring a host's ability to recognize, target, and destroy tumors has opened a promising avenue of research for cancer therapy. This is particularly the case in metastatic tumors, since the ability of these tumors to spread is dependent heavily on remaining unrecognized by the immune system (Dong et al., 2002; Drake et al., 2006; Kusmartsev and Gabrilovich, 2006; Hinz et al., 2007). Tumors that express *PDL1* are prime candidates for PD1-mediated treatments, yet some tumors remain immune resistant. Recalcitrance to these therapies could be due to their genetics (e.g., immune evasion), mutational burden, or physical location.

In this light, immune evasion can conceptually be thought of as an inversion of autoimmunity. In autoimmunity, a host's immune system becomes "hyperactive," or the target tissue becomes immunoreactive, and the immune system aberrantly recognizes the host's own tissues as foreign antigens. The immunological pathways activated in some autoimmune diseases, such as alopecia areata (e.g., cytotoxic $CD8^+$ T cell activation), are the same pathways that are inactivated in cancers (Dunn et al., 2002; Xing et al., 2014; Chen et al., 2015). In light of this, we propose a strategy for enhancing cancer immunotherapy that entails "hijacking" the molecular mechanisms that activate the immune system in autoimmune disease and using them to essentially "tag" evasive tumors for immune-mediated destruction. We reasoned that the molecular processes that encourage active immune cell infiltration to the target organs in autoimmune disease could be used to restore immune targeting against cancer cells.

Previously (Chen et al., 2015), we demonstrated that the master regulator *IKZF1* is sufficient to induce the recruitment of immune infiltrates that result in immune-mediated cytotoxicity seen in autoimmunity when expressed in target tissues. Exogenous overexpression of *IKZF1* was sufficient to induce autoimmune susceptibility in unaffected cultured cells primarily through infiltrating $NKG2D^+$, $CD8^+$ T cells. Based on these findings, we hypothesized that tumor cohorts may achieve immune evasion via *IKZF1*-inactivating mutations. These tumors would then be susceptible to enhancement therapy through the restored expression of *IKZF1*. In this study, we sought to computationally

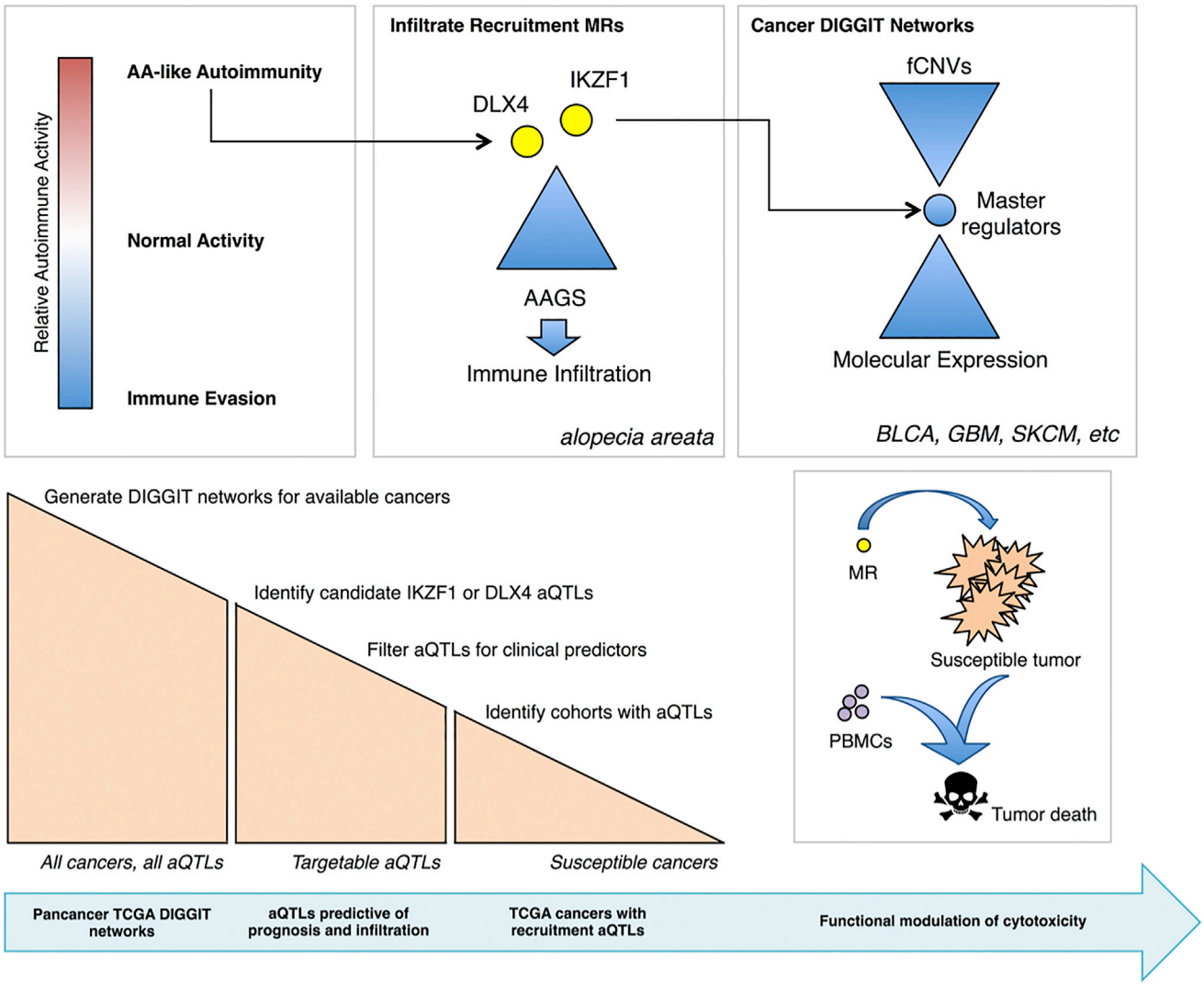

Figure 1. Schematic Flow Detailing How Master Regulators and Regulatory Networks Can Be Used to Identify Targetable Cancer Cohorts for Enhancement of Immunotherapy

Previous work in autoimmune diseases has identified immune pathways that are both activated in autoimmune disease and suppressed in cancers, providing the hypothesis that co-opting immune-recruitment signals in autoimmune disease may be beneficial in mediating immunotherapies. The validated master regulators, *IKZF1* and *DLX4*, govern enhanced immune infiltration in alopecia areata, and DIGGIT is capable of screening cancer patients for the presence of these master regulators in their genetic-genomic networks and analyzing them for association with clinical outcomes and predictors. Tumors with these master regulators become candidates for enhancement of immunotherapies through supplementation of these master regulators.

identify cancer cohorts whose genetic-genomic architecture (Chen et al., 2014) included *IKZF1* disruptions, to validate the ability of *IKZF1* to rescue or induce cytotoxic immune interactions in these tumors and to assess the enhancement of immunotherapy efficacy.

RESULTS

Network Analysis Identified Cancer Cohorts Amenable to Enhancement of Checkpoint Inhibitor Therapy

The overall framework for this pipeline is detailed in Figure 1. In theory, systems biology-based analytics using regulatory networks can infer the master regulators of any modular complex trait associated to a well-defined gene-expression signature. Due to the significant relevance of immunotherapies for cancer treatment (Ascierto et al., 2010; Min and Hodi, 2014; Rizvi et al., 2015; Valecha et al., 2017; Godfrey et al., 2017) and our previous identification of master regulators activating immune infiltrate recruitment in autoimmune disease (Chen et al., 2015), we postulated that certain tumors might acquire immune evasion through the suppression of such master regulators. With access to regulatory and DIGGIT (Chen et al., 2014) networks of 15 cancers provided by The Cancer Genome Atlas (TCGA) (Verhaak et al., 2010), we sought to identify and validate patient cohorts that may be amenable to immune enhancement by identifying patients with a functional *IKZF1* regulon and driver mutations in their regulatory networks.

Patients with *IKZF1* disruptions can be computationally identified using integrated regulatory network algorithms (DIGGIT). This algorithm defines "activity quantitative trait loci" (aQTL) in patient tumors that are predicted to disrupt the activity of specific master regulators. This is achieved by reconstructing genetic-genomic interaction networks from patient-matched data to identify functional alterations in the genome that coincide with molecular disruption of master regulators, the particulars of which are detailed in previous publications (Chen et al., 2014; Califano, 2014) and detailed in STAR Methods. In brief, the algorithm sorts through genomic mutations and assigns them functions based on whether or not they perturb the molecular behavior of a master regulator through an accompanying gene-expression regulatory network.

Therefore, we can leverage the aQTL networks across the TCGA cancer cohorts to identify cancer subsets that have functional alterations in *IKZF1*. A positive prediction by this approach indicates that (1) *IKZF1* is a functional master regulator in a tested tumor, and (2) there is genomic evidence that the activity of *IKZF1* is perturbed. These cancer types should therefore be tested for susceptibility to immune modulation via these master regulators. We postulated that if an aQTL for the *IKZF1* regulon exists, then regulatory logic exists within the corresponding patient cohort that can potentially phenocopy the recruitment of immune infiltrates. These cancers were subsequently selected for more in-depth study and validation.

Eight TCGA Cancers Have Targetable IKZF1 aQTLs

We interrogated a total of 15 DIGGIT networks corresponding to the available TCGA tumor cohorts: cutaneous melanoma (SKCM), glioblastoma (GBM), head-and-neck squamous carcinoma (HNSC), lung adenocarcinoma (LUAD), thyroid carcinoma (THCA), bladder carcinoma (BLCA), lung sarcoma (LUSC), prostate adenocarcinoma (PRAD), uterine corpus endometrial carcinoma (UCEC), kidney/renal carcinoma (KIRC), colorectal adenocarcinoma (COAD), rectal adenocarcinoma (READ), liver hepatocellular carcinoma (LIHC), low-grade glioma (LGG), and stomach adenocarcinoma (STAD). For each network, we tested specifically for aQTLs enriched in the validated *IKZF1* regulon that confers immune susceptibility in alopecia areata, which primarily governs the infiltration of $CD8^+$ $NKG2D^+$ cytotoxic T cells (Chen et al., 2015). The DIGGIT networks themselves were built using corresponding TCGA datasets using the standard published pipeline (Chen et al., 2014), false discovery rate (FDR) < 0.05. The overall distribution of enrichment in each tumor can be used to ascertain whether or not the regulatory and genomic network architecture of these tumors includes the candidate master regulators. Those tumors that do contain such aQTLs are potentially susceptible to immune modulation through *IKZF1* as a master regulator.

The results for the DIGGIT analysis of *IKZF1* are presented in Figure 2. For each tumor, the distribution of p values in the top 100 candidate aQTLs are presented (Figure 2A) in addition to a median null distribution of aQTLs defined by bootstrapping randomized gene signatures (see STAR Methods). The complete distributions represented as box-and-whisker plots are also available as Figure S1. The divergence between these two distributions was tested statistically using the non-parametric Mann-Whitney U test. The TCGA STAD cohort was omitted entirely due to an inability of the algorithm to achieve sufficient aQTL resolution.

Using this as a metric, eight cancer types were identified as having IKZF1 aQTLs: SKCM, GBM, HNSC, THCA, LUAD/LUSC, PRAD, and BLCA (FDR < 0.05).

IKZF1 Expression Induces Immune-Mediated Cytotoxicity Molecular Programs

Based on the DIGGIT analysis, we obtained seven human-derived tumor cell lines corresponding to the cancers bearing *IKZF1* aQTLs (GBM, THCA, SKCM, PRAD, BLCA, and LUAD). Each cell line was stably transduced with an RFP (negative control) and *IKZF1* constitutive-expression construct. We subsequently cultured the stable lines for use in immune-mediated cytotoxicity assays (Chen et al., 2014) using peripheral blood mononuclear cells (PBMCs) isolated from human whole-blood samples. This assay measures the relative cell death of a target cell population after exposure to immune cells, and can be used to test the hypothesis that the induction of *IKZF1* will enhance tumor cell susceptibility to immune-mediated cytotoxicity. Following 8 hr of co-incubation, we observed statistically significant increases in immune-mediated cytotoxicity in *IKZF1*-transfected cells compared with their corresponding RFP controls by t test ($p < 0.05$, Figures 2B and 2C). This was true of five of the seven lines tested: two SKCM lines, GBM, THCA, and PRAD. Conversely, the BLCA and LUAD lines tested failed to demonstrate a significant enhancement of immune-mediated cytotoxicity. These results are ranked by absolute fold change (*IKZF1* versus matched *RFP*).

These cell lines were then sent for gene-expression profiling via RNA sequencing (RNA-seq). We tested each cell line for enrichment of the validated IKZF1 immune-recruitment regulon (Chen et al., 2015) as a measure of functional relevance using gene set enrichment analysis (GSEA) (Subramanian et al., 2005). Figure 2D details the results of each GSEA. Across all available cell lines, the transduction of *IKZF1* resulted in statistical enrichment of the *IKZF1* immune-recruitment regulon compared with RFP counterparts at FDR < 0.05 (Subramanian et al., 2005), indicating that the DIGGIT-predicted tumor cohorts in fact contain the regulatory logic associated with our characterized *IKZF1* aQTL, and thus may be amenable to the rescued expression of *IKZF1* to enhance immune infiltrate recruitment.

IKZF1 Expression in Mouse-Derived Melanomas Suppresses Melanoma Growth

Since the human melanoma (SKCM) TCGA cohort had the most significant candidate driver predictions across the entirety of this network analysis (the strongest DIGGIT aQTLs, correlations with prognosis, and with immune infiltration marker panels), we turned to a syngenic melanoma model using C57/B6 mice to perform *in vivo* characterization of the role of *IKZF1* as a master regulator of immune-recruitment enhancement. B16F10 spontaneous melanomas are isolated from immunocompetent mice and can be reintroduced as oncogenic subcutaneous grafts in the C57/B6 background via subcutaneous injection. This tumor line does not normally express *IKZF1* (see Figure S2A), making it ideal for testing overexpression of *IKZF1*. We cultured B16F10 tumor cells and stably transduced a constitutively active

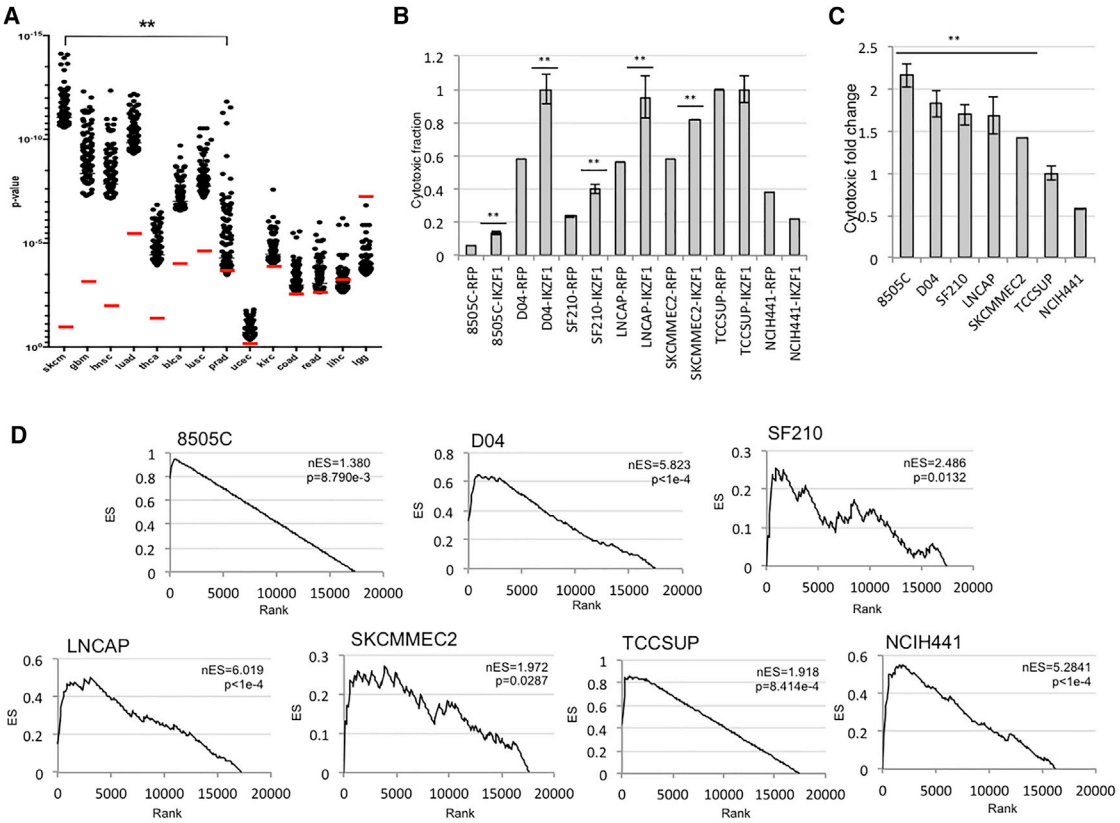

Figure 2. Computational Analysis of TCGA Cohorts for *IKZF1* aQTLs and *In Vitro* Validation of the Regulon

(A) The top 100 candidate aQTLs (black dots) for each tested cancer from TCGA that are predicted to affect *IKZF1* regulator activity. p values (FDR corrected) reflect the statistical enrichment of the aQTL for the validated *IKZF1* regulon in each cancer. The red hashes denote the median values for 10,000 bootstrapped null distributions. Significance (**) is defined by having both statistical divergence between the top 100 candidates and the null distributions, and surpassing $p = 1 \times 10^{-5}$.

(B) *In vitro* validation of immune enhancement in seven human tumor lines representing the significant computational predictions. Each cell line was stably transfected for exogenous expression of either *IKZF1* or *RFP* (negative control). The y axis reflects the total cytotoxic fraction incurred upon introduction of whole-blood PBMCs. Significance (**, FDR < 0.05) denotes that a statistically significant difference in cytotoxic fraction was observed between case and control pairs.

(C) Normalized representation of data in (B) Each *IKZF1* transfection is normalized to its *RFP* control.

(D) GSEA analysis of RNA-seq data for these tumors shows statistically significant enrichment of the validated *IKZF1* regulon in all tested lines. Data are plotted as the mean ± SEM.

IKZF1 construct (or *RFP* control). We grafted 5×10^4 cells into B6 mice and tracked the development of tumors over 21 days (Figure 3A). We observed a statistically significant reduction in tumor size in mice grafted with IKZF1-producing B16F10 tumors as compared with the RFP controls. The difference in tumor growth was detectable as early as 17 days post graft and was stable until the end of the time course. Conversely, there was no significant reduction in growth when this experiment was conducted in immunocompromised nude mice (Figure S2B), indicating that an active immune system is necessary for the tumor-suppression phenotype. Viability of the mice was not affected by the injections except one, which was excluded from analysis (Figure S2C).

We performed *in vitro* cytotoxicity assays using PBMCs isolated from whole blood of individual mice against both *IKZF1*- and *RFP*-B16F10 to quantify IKZF1-dependent immune-mediated toxicity. Upon completion of the time course, whole blood was isolated from three *RFP*- and four *IKZF1*-grafted mice. PBMCs were isolated for cytotoxicity assays using the B16F10 stably transfected cells (Figure 3B). PBMCs from each mouse were tested against both *IKZF1*- and *RFP*-transduced cells, and in six of seven samples there was a statistically significant increase in immune-mediated cytotoxicity in *IKZF1* tumors compared with *RFP* controls. The last sample exhibited a notable and concordant increase, but fell marginally short of statistical significance by t test (FDR < 0.1 but $p < 0.05$).

Taken as a whole, there was a statistically significant increase in immune-mediated cytotoxicity in *IKZF1*-B16F10 cells compared with *RFP* controls ($p = 2.79 \times 10^{-4}$). This effect was not dependent on the PBMC source (whether the PBMC donor initially received an *IKZF1* or *RFP* xenograft). Instead, the only predictor of increased immune activity was whether or not the tumor itself expressed *IKZF1*.

Increased CD8$^+$ T Cell Infiltrates Found in B16F10 Grafts with IKZF1 Expression

After the completion of the time course, we collected the remaining tumors and performed RNA-seq profiling to quantify the

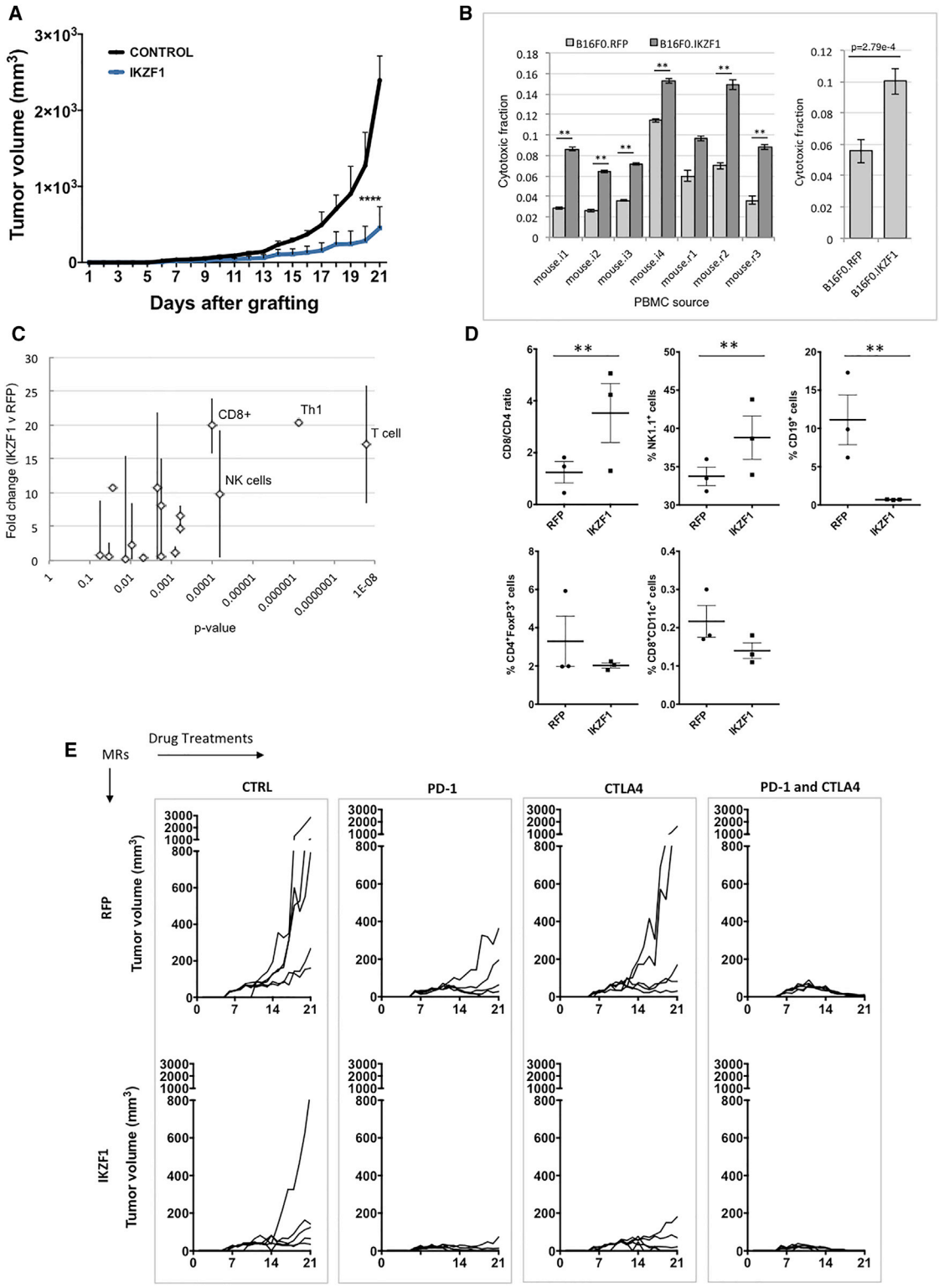

Figure 3. Results of a Syngenic Melanoma Mouse Model Testing Immune-Recruitment Enhancement Function of IKZF1

(A) Composite (n = 5 per arm) tumor growth curves of B16F10 melanomas in a syngenic, immunocompetent B6 mouse background. Tumors were stably transfected with either *RFP*- or *IKZF1*-expressing constructs and subcutaneously injected into mouse flanks. Tumor growth was recorded over the course of 21 days. There was a statistically significant separation in tumor growth solely based on the expression of *IKZF1* (****$p < 0.01$).

(legend continued on next page)

molecular effects of *IKZF1* transduction. We quantified the relative abundance of infiltrating immune cells within the tumor mass based on the RNA-seq consensus of each immune cell type, each defined by a unique molecular biomarker panel derived from tumor infiltrate studies (Bindea et al., 2013; Jabbari et al., 2016). These panels were cross-checked with the gene-expression profiles of ungrafted, *in vitro* cultured tumors to ensure exclusivity (provided in Supplemental Information). Figure 3C displays the consensus fold change of each immune cell type and the p value associated with it following Fisher's integration. In particular, four categories of immune markers—T cell markers, T helper type 1 (Th1) markers, natural killer (NK) cell markers, and $CD8^+$ markers—were at least one order of magnitude more statistically significant than the others, as well as displaying an average 10- to 20-fold change increase in *IKZF1*-treated tumors. These markers were all highly increased in *IKZF1*-expressing tumors, suggesting selective increases in infiltration of these specific immune cell populations in the tumors. We included *in vitro* cultured *IKZF1* and *RFP* B16F10 cells as negative controls, and these samples did not register any reads to these markers, indicating that these cells reflect immune infiltrates from the mouse host (Tables S2 and S4).

These results were confirmed at the protein level by flow-cytometry analyses. Post-treatment residual tumors were excised and processed for flow (see STAR Methods) to quantify the relative $CD8^+$ immune cell infiltrate. Cells were stained for CD4 and CD8; in these studies we observed an approximately 3-fold enrichment of $CD8^+$ cells ($p < 0.05$) in the infiltrate in IKZF1-expressing tumors compared with the corresponding RFP controls (Figure 3D). Paired t test analysis of the CD8 and CD4 populations independently also indicated statistically significant increases in $CD8^+$ cells ($p < 0.03$) and CD4 cells ($p < 0.02$). We additionally analyzed markers for T regulatory cell populations (FOXP3), B cells (CD19), NK cells and $CD8^+$, NK cells (NK1.1), and dendritic cells (CD11c). There were statistically significantly elevated levels of $NK1.1^+$ cells, as a significant suppression of $CD19^+$ cells in the extracted infiltrates.

IKZF1 Expression Suppresses Tumor Growth in Combination with α-PD1 and α-CTLA4 in Melanoma

While the previous experiments established the mechanistic relevance of *IKZF1* as a master regulator, we sought to further investigate its potential translational implications. We repeated the mouse experiments, this time incorporating individual and combinatorial treatments of α-PD1 and α-CTLA4 antibodies (Figure 3E). Photos of mice from each arm are provided in Supplemental Information. The quantification of tumor mass is also provided in linear and logarithmic scale (for improved resolution of the smaller tumors). Administration time points of α-PD1 and/or α-CTLA4 is indicated by arrows at the provided dosages.

Over the 21-day time course, we observed that *IKZF1* expression was sufficient to phenocopy the kinetics of PD1 inhibition, such that they are statistically indiscernible (both are statistically significant from controls at $p = 0.05$). Individual CTLA4-inhibitor treatment had no statistically differentiable effect on tumor growth, but was enhanced by *IKZF1* expression. Combinatorial therapy of PD1 and CTLA4 inhibitors resulted in the eventual suppression of tumor growth, but this was not observable until post-graft day 14. Notably, any combination of *IKZF1* overexpression with a drug treatment regimen significantly enhanced the regression rates of B16F10 growth, and tumors began following a regressive curve as early as 8 days post graft compared with RFP controls. In particular, α-CTLA4 treatment alone was largely ineffective compared with controls, but produced a significantly enhanced effect when combined with *IKZF1*. Inclusion of *IKZF1* treatment with both α-PD1 and α-CTLA4 resulted in complete tumor regression by day 18, and significantly enhanced the rate of regression throughout the entire time course compared with α-CTLA4 and α-PD1 alone. Composite data plots in linear and log scale for each treatment are available in Figure S2D, with representative photos shown in Figure S2E.

IKZF1 Immune Rescue Is Validated in Three Additional Mouse Cancer Lines

As a final *in vivo* test of both the positive and negative predictive value of the computational approach, we repeated the mouse model experiments in two tumor models that we predicted would be recalcitrant to *IKZF1*, renal (READ/RENCA), and colorectal (COAD, CT26) tumors, as well as a second model predicted to be sensitive to *IKZF1*, prostate (PRAD, MyC-CaP). READ and COAD were shown by the DIGGIT analysis to either have unmutated or inactive (unexpressed) *IKZF1* in their genetic-genomic networks, suggesting that introduction of *IKZF1* would have minimal effect. Conversely, PRAD showed statistically enriched aQTLs disrupting *IKZF1* activity, and our *in vitro* assays in human lines suggested that *IKZF1* expression would enhance infiltration in a manner similar to SKCM. Our experiments validated our predictions in both scenarios: the prostate tumors recapitulated the results observed with the B16F10 line (Figure S3, left panels), and were only observed in immunocompetent mice (Figure S3, right panels). We were able to recapitulate the effectiveness both of *IKZF1* independently and in combination with PD1 and

(B) *In vitro* cytotoxic killing experiments using the B16F10 tumors and whole-blood PBMCs isolated from seven mice in the trial: four receiving *IKZF1* tumors and three receiving *RFP* tumors. Six of seven comparisons demonstrated statistically significant enhancement of immune-mediated cytotoxicity when *IKZF1* was expressed within the target tumor, and with no association or dependence on the tumor that the blood-donor mouse received (**$p < 0.05$).

(C) RNA-seq analysis of remaining tumor masses after the time course for the presence of immune infiltrates. Immune infiltrate consensus signatures were used to quantitate the relative presence of each immune type. The x axis represents the overall statistical significance of the signature's enrichment in *IKZF1*-expressing tumors compared with their corresponding *RFP* controls. The y axis reflects the overall fold change difference. T cell, Th1, CD8-positive, and NK cell signatures passed the set threshold of 1×10^{-4} and at least 2-fold difference.

(D) Flow-cytometry analysis of remaining tumors for immune infiltrates including $CD4^+$ cells (CD4), $CD8^+$ cells (CD8), T regulatory cells (Foxp3), B cells (CD19), NK and CD8NK cells (NK1.1), and dendritic cells (CD11c). Asterisks denote statistically divergent populations (**$p = 0.05$).

(E) Immunotherapy enhancement experiments repeated using transfected B16F10 tumors in combination with PD-1 inhibitors, CTLA4 inhibitors, or both. Graphs denote individual tumor growth rates over 21 days in *RFP* (top row) tumors or *IKZF1* (bottom row) tumors alone, and with each inhibitor combination (columns). Composite data are plotted as the mean ± SEM.

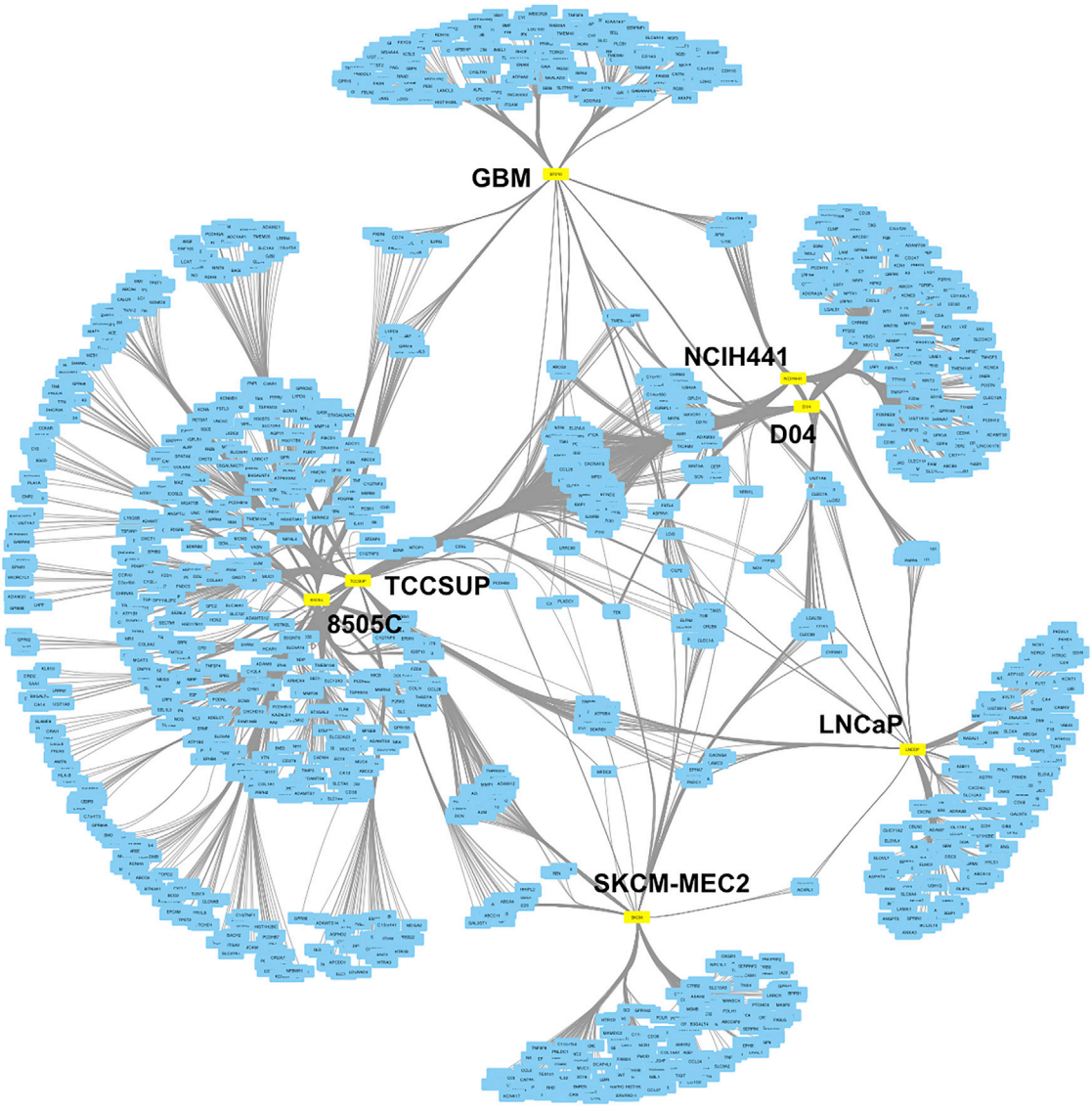

Figure 4. Map of *IKZF1*-Dependent Alterations in Signaling and Membrane-Bound Molecules in Tested Human Tumor Lines

All tumors demonstrated extensive reorganization of signaling molecules following *IKZF1* expression compared with corresponding *RFP* controls (full list is available in Supplemental Information). 8505C and TCCSUP, as well as NCIH441 and D04, showed similar profiles of reorganization despite being differently originating tumor types.

CTLA4 inhibitors in PRAD. In contrast, both the READ and COAD tumor lines failed to suppress tumor growth individually (*IKZF1* only) or enhance PD1 and CTLA4 inhibition. Taken together, these *in vivo* studies bring the predictive accuracy of the algorithm to 2/2 positive and 2/2 negative.

IKZF1 Overexpression Induces Significant Changes in Expression of Immune Markers in Human Tumors

Since our data indicated the overall activation of immune infiltrate recruitment signals, we returned to the RNA-seq data of the human tumors lines (first described in Figure 2, available in Table S2) and tested for an association of *IKZF1* overexpression and subsequent changes in cytokine or membrane-bound signaling molecules. This was defined by comparing each *IKZF1*-transfected line to its respective *RFP* control, taking all genes that were differentially expressed by at least 20% and performing naive functional annotation enrichment analysis. This was done independently for each tumor type and the results were integrated for comparative viewing in Figure 4. Blue nodes represent individual genes that were differentially expressed, and linked yellow nodes denote the cancers in which association was detected. The differential expression profiles of all tumors tested were significantly enriched in membrane-bound signaling molecules ($p < 1 \times 10^{-20}$ corrected), as well as in immunoglobulin, immune response, immune activation, and cytokine annotation categories ($p < 1 \times 10^{-10}$ corrected). This list includes human leukocyte antigen, interferon, and chemokine signature genes, a full list of which is available in Table S3. The overall

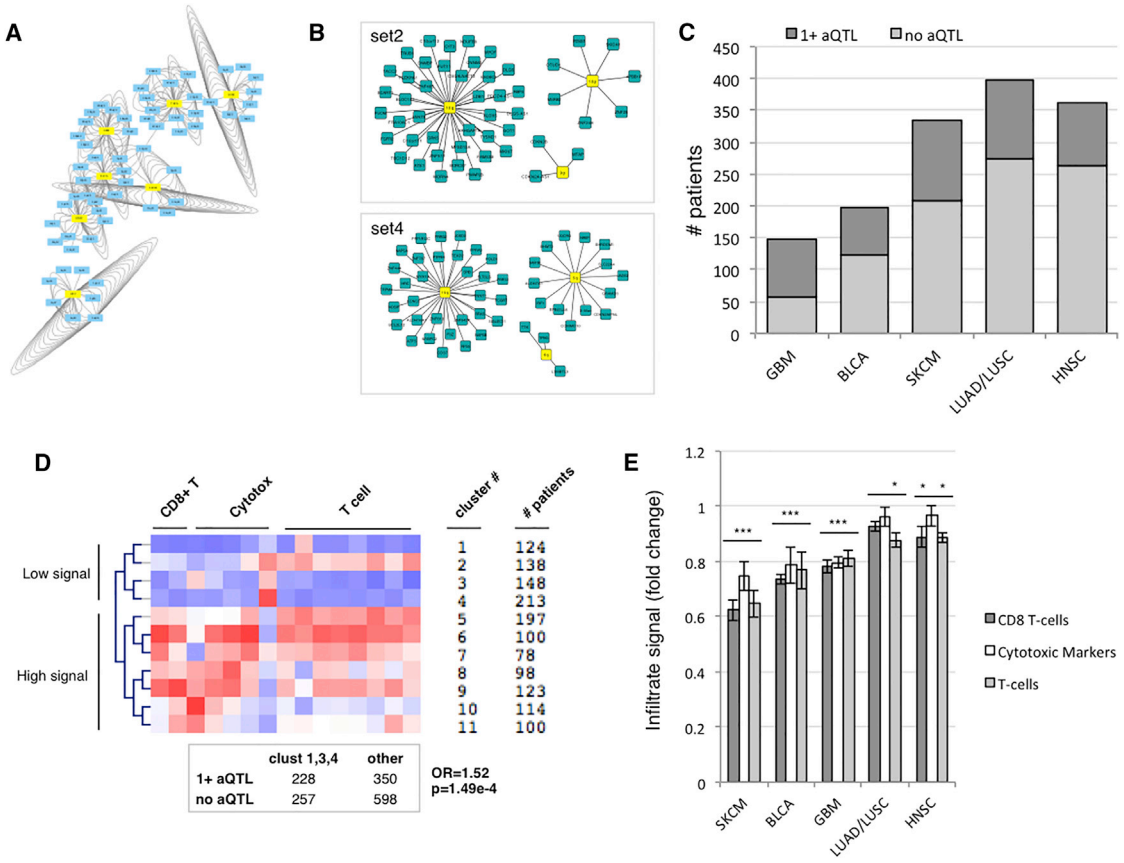

Figure 5. Immune Infiltrate Detection Studies in Human Cancer Cohorts Using *IKZF1* as a Biomarker

(A) DIGGIT analysis maps the most significant genomic aQTLs that affect IKZF1 activity in each positively predicted tumor from TCGA. Certain genomic regions are shared between tumor types.

(B and C) Two sets of aQTLs were most closely associated with clinical predictors (B), and human patients with CNVs in these regions account for ~30%–50% of samples in these cohorts (C).

(D) Repeating immune infiltration analysis with this independent cohort naively identifies 485 patients with low $CD8^+$ and T cell signatures (clusters 1, 2, and 4). There is statistically significant enrichment of these 485 patients for mutations in the two candidate sets of *IKZF1* aQTLs (see table).

(E) Quantification of raw infiltrate levels in these cohorts comparing patients with and without aQTL mutations demonstrates statistically significant suppression of immune infiltration levels in patients who bear *IKZF1*-affecting CNVs (* denote tests $p < 0.05$ per set of cell types, e.g., *** indicates all three tested types are significant). Data are plotted as the mean ± SEM.

description, commonalities, and divergence in the effects of *IKZF1* on the expression of these genes across the cancer types can be seen in Figure 4. This analysis details the molecular enrichment of immune markers associated with *IKZF1* expression in human tumors, providing insight into how the master regulator may mediate an increase in immune-mediated cytotoxic sensitivity.

Genomic Alterations in IKZF1 aQTLs Are Predictive of Decreased Immune Infiltrates in TCGA Human Cancer Cohorts

In this study, the application of DIGGIT to 15 cancer cohorts from TCGA identified the presence of targetable master regulators using a combination of transcriptional networks and genomic mutation architecture. Copy-number variations (CNVs) were used as the primary genomic feature. The algorithm predicts genomic mutations that drive aberrant master regulator activity by linking specific CNVs to coordinated regulatory changes through a network. These fCNVs (functional CNVs) can be clustered into co-mutated loci that reflect typical minimal-common-regions of mutations that are observed in human patients (Chen et al., 2014). This effectively creates small numbers of mutation sets that can be used as biomarkers for association studies in human cohorts (Figure 5A). In this instance, we identified two sets of mutations in the affected cohorts (Figure 5B), accounting for 30%–50% of patients in each tumor cohort (Figure 5C). The frequency of the *IKZF1* aQTL in these tumors is conducive to an immune infiltrate analysis (>10% of patients for sufficient statistical power). By segregating patients into subgroups based on whether or not an individual had evidence of genomic alterations that affect master regulators of immune infiltrate recruitment, genomic disruptions of IKZF1 can then be tested for association of molecular and physiological outcomes.

We therefore aimed to establish an association between tumor immune infiltration and mutations in *IKZF1* aQTLs under the hypothesis that tumor samples bearing such mutations will

have lower levels of infiltrating signal. Since our primary interest in *IKZF1* is as a recruiter of $CD8^+$ $NKG2D^+$ T cells (Xing et al., 2014; Chen et al., 2015), we extracted the appropriate CD8, T cell, and cytotoxic marker signatures from Bindea et al. (2013) and performed a naive random forest clustering across these patients to ascertain whether or not a difference in these signatures was detectable. The clustering identified ten partitions (11 total clusters) based on the Bindea signatures for these three marker panels (Figure 5D) that could be organized into patients with high and low signals of immune infiltration. Using this classification, we detected a statistically significant enrichment of patients bearing *IKZF1* aQTLs in the three lowest pan-signal clusters (1, 3, and 4), odds ratio = 1.52 and $p = 1.49 \times 10^{-4}$ by Fisher's exact test. Cluster 2 was included in the high-signal group due to the abundance of T cell markers, despite the relative lack of CD8 and cytotoxic markers. This result indicates that patients with fCNVs affecting *IKZF1* are significantly more likely to have the lowest levels of immune infiltrate signal (a complete description of all immune types is available in Figure S4 and Table S5).

The difference in immune infiltrate levels was quantified using gene expression across each of the cancers by relative fold change (Figure 5E). Normalized fold changes show statistical changes in individual immune marker panels. The SKCM, BLCA, and GBM cohorts demonstrated the most significant shifts in all three immune marker panels, while LUAD/LUSC and HNSC showed statistically significant changes in CD8 and T cell markers. These results suggest that the candidate aQTL loci have the strongest evidence for influencing immune infiltration in the SKCM, GBM, and BLCA cohorts.

Decreased IKZF1 Activity Predicts Recurrence and Poor Prognosis in an Independent Cohort of Human Melanoma and across TCGA Cancer Cohorts

We analyzed an independent clinical melanoma cohort with expression data (Sivendran et al., 2014) for immune infiltrates to analyze the predictive value of *IKZF1* expression. These samples were assayed for immune markers and correlated to clinical response and recurrence rates. In this case, comparative analysis was done by binning the patients in order of *IKZF1* expression and comparing the upper and lower 30% against each other. In this comparison, we found that decreased *IKZF1* expression was significantly associated with tumor recurrence (FDR < 0.05, Figure 6A), and was also predictive of overall suppression in detectable infiltrates measured by immune biomarker panels (Figure 6B).

Returning to the TCGA datasets, we segregated all patients into two cohorts defined by whether or not each patient had CNVs affecting *IKZF1* activity as previously defined (set 1, Figure 6C and set 2, Figure 6D). Cohorts of CNV-bearing patients were tested against their corresponding negative control cohort (no CNVs) for various clinical survival outcomes. Across all tests, we found that patients with CNVs in at least one gene within these loci presented with significantly shorter median survival and higher mortality rates than patients with no mutations at these loci. The set of genes (listed in Supplemental Information) that are directly linked to *IKZF1* activity and decreased immune infiltration are also sufficiently predictive of poor prognosis regardless of any other mitigating factor. They represent the most clinically relevant candidate loci that perturb the *IKZF1* regulon, and therefore serve as both genomic indicators of susceptibility to *IKZF1* modulation and ideal candidates for further functional studies and drug discovery.

DISCUSSION

An analysis of DIGGIT networks across the TCGA data was able to identify patient subsets across six cancers that display significant evidence of *IKZF1* aQTLs. While straightforward, this result has two key corollaries. First, it indicates that a genomic alteration can be functionally linked specifically to the molecular behavior associated with regulation of infiltrate recruitment in cancer cohorts (identifying immunoreactive versus immune-resistant tumors). Second, it provides an actionable target for enhancement of immune therapies (converting immune-resistant tumors to an immunoreactive state).

In terms of translational applications, these findings add to a growing body of literature proposing master regulators not only as biomarkers of important pathophysiology, but also as targets for drug therapy development. *IKZF1* is a key regulator of a complex molecular signature governing immune infiltrate recruitment, making it both a predictor of response to therapy and an excellent candidate for future drug targeting. Computational modeling of drug mechanism of action using similar analytic pipelines allows for the matching of compounds to patients based on the key master regulators governing their particular molecular pathologies (Woo et al., 2015), allowing for the possibility of identifying patients with cancers bearing *IKZF1*-inactivating mutations and planning treatments accordingly, e.g., combinatorial therapy with a compound that activates the *IKZF1* regulon.

Here, we showed that five of seven (GBM, two different SKCM, PRAD, and THCA) tested tumor types that were predicted to be responsive to IKZF1 therapy (immune-reactive tumors with *IKZF1* in their regulatory logic) did indeed respond in *in vitro* assays with a physiologically observable output (increased cytotoxicity). The results of this study draw parity between GBM and SKCM cancers, which are usually considered disparate using more classical oncological definitions. This finding suggests that cancers traditionally considered completely disparate may have common therapeutic targets from a regulatory perspective. The RNA-seq analysis and *in vitro* assays demonstrate that *IKZF1* expression in the tumor masses enhances immune infiltration, supporting the predictions drawn by our network analysis.

The overexpression of a single master regulator was sufficient to induce the activation of a complex immune infiltrate recruitment signature (Chen et al., 2015) across several predicted tumor types, resulting in enhanced molecular interactions with cytotoxic immune cells. This in turn identifies *IKZF1* as the minimum regulator required to coordinate a complex molecular phenotype (Margolin et al., 2006; Lefebvre et al., 2010), and makes for an ideal candidate for further mechanistic studies. It should be noted that one predicted cell line, TCCSUP, demonstrated no clear statistical shift in the *in vitro* immune-mediated cytotoxicity assays. This could be due to unidentified mutations downstream of *IKZF1* in the signaling pathway, or an

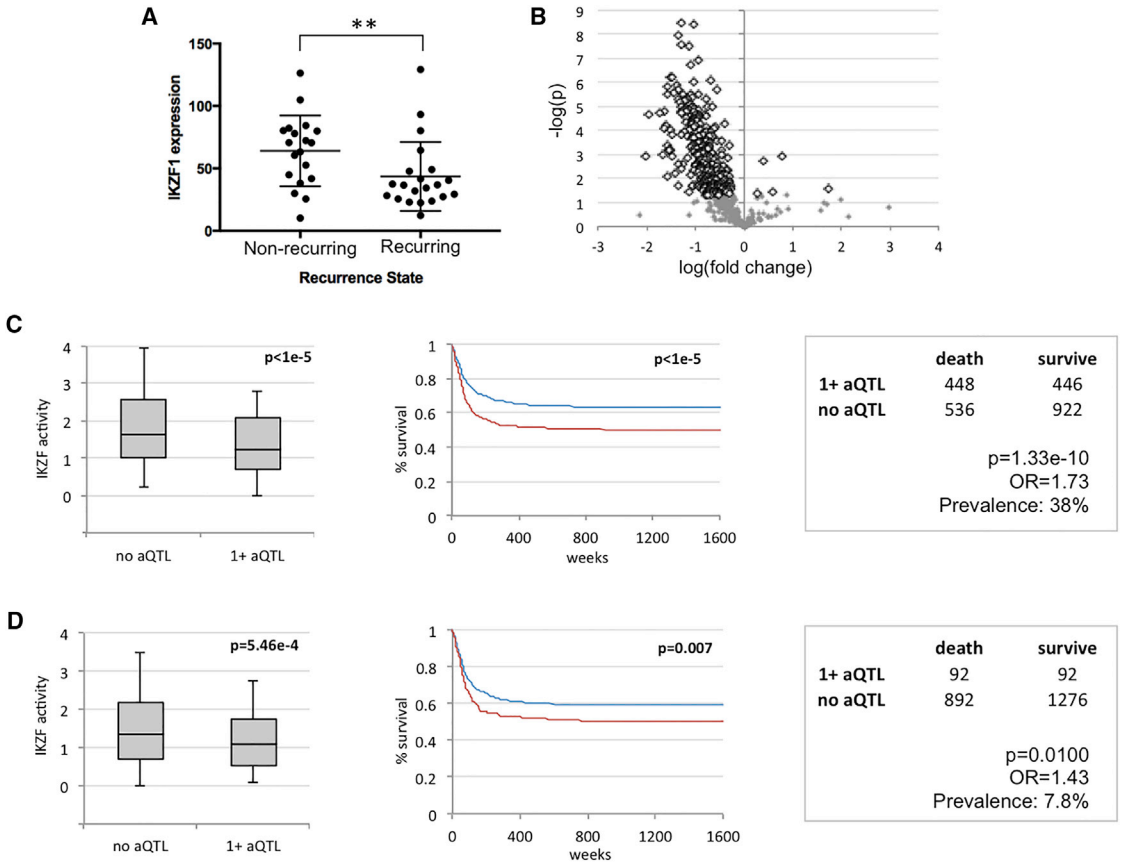

Figure 6. Prognostic Studies in Human Cancer Cohorts Using IKZF1 as a Biomarker

(A) An independent human melanoma cohort aimed at studying recurrence rates shows that recurring tumors are statistically associated with lower levels of *IKZF1* expression (**$p < 0.05$).

(B) Patients in the cohort with low *IKZF1* expression associate with overall significant suppression of infiltrate biomarker panels (red dots).

(C and D) In TCGA patients, and across all available cancers, CNVs in the candidate aQTLs (C, set 2; D, set 4) predict suppression of *IKZF1* activity, and are solely sufficient to predict poor clinical outcomes by Kaplan-Meier prognostics (red line, mutation bearing aQTLs; blue line, no mutations) and by overall total survival rates. Data are plotted as the mean ± SEM.

insufficiency of the *in vitro* assay to reflect the necessary biological conditions to elicit a measurable response. NCIH441 responded with a suppression of tumor immune sensitivity. While this is clearly not ideal from a clinical treatment perspective, the network analysis sufficiently identified that *IKZF1* was a functional node in the regulatory network—the analysis was not conducted to include directionality in the molecular predictions.

These results translated into the syngenic mouse melanoma model. Stably transfected *RFP* and *IKZF1* B16F10 tumor cells were maintained on low-level selection, sorted by fluorescence-activated cell sorting, and grafted into the appropriate strain of immunocompetent B6 mice. Across all experiments there was a statistically significant separation in tumor growth detectable as early as 15–16 days post injection. Importantly, this was not observed when the experiment was repeated in immunocompromised nude mice. The statistically inseparable survival outcomes of *IKZF1*- and *RFP*-expressing melanomas in nude mice suggested that an active immune system is necessary for the suppression phenotype.

These experiments also demonstrated that the function of these master regulators is mediated through the tumor itself, rather than the accompanying host immune system. This is evidenced by the identification of somatic driver mutations throughout the TCGA cohorts as well as the exogenous *IKZF1* expression restricted entirely to the tumor, and is further supported by the *in vitro* cytotoxicity assays. Across all trials, the trend was the same: the defining predictor of enhanced cytotoxicity was whether or not the melanoma itself expressed *IKZF1*; whether or not the PBMCs had been previously exposed to an *IKZF1* tumor was irrelevant.

From a translational perspective, *IKZF1* expression in melanomas provided synergistic enhancement of both α-PD1 and α-CTLA4 inhibition. This observation adds to the growing body of research suggesting the promise of leveraging master regulators to drive novel clinical and therapeutic development. *IKZF1* exogenous expression alone is sufficient to phenocopy the tumor suppression following PD1 inhibition, and facilitates efficacy of CTLA4 inhibition that is not observed in individual treatment. Although the effect size of PD1 treatment itself

extends to about 10% of patients, DIGGIT analysis of TCGA cancer cohorts identifies approximately 20%–40% of patients across six cancer types as carrying *IKZF1* aQTLs. This result suggests that these treatments may be applicable to a significantly larger number of patients via master regulators governing local immune infiltrate recruitment.

This is further corroborated by the subsequent RNA-seq analysis. We observed statistically significant, elevated consensus levels of infiltrating $CD8^+$, T cell, Th1 cell, and NK cell populations uniquely in the mouse tumors expressing *IKZF1*. These are the primary cell types that were originally implicated in alopecia areata pathology via these same master regulators (Xing et al., 2014; Chen et al., 2015) and reflect the same molecular pathways that have been reported as suppressed in cancer. This analysis provides compelling evidence of the specificity of these master regulators, since only these select populations were significantly enriched as infiltrates in the IKZF1 tumors.

Finally, demonstrating both the positive and negative predictive values of these approaches, we showed that two cancer types that we predicted to be completely non-responsive to *IKZF1* expression showed no response to overexpression in *in vivo* mouse models. CT26 (COAD) and RENCA (READ) were predicted by network analysis not to have *IKZF1* as a functional or relevant regulator. In functional mouse models, we observed that exogenous expression of *IKZF1* in these tumors indeed had no effect on tumor growth or aggressiveness independently, nor did they enhance the efficacy of PD1 or CTLA4 inhibitors. Across TCGA cancer cohorts and an independent melanoma cohort, disruptions of the *IKZF1* regulon were sufficient to predict poor prognosis, high mortality rates, and recurrence of tumors.

On a broader scale, this work also demonstrates the feasibility of using systems biology approaches to drive the discovery of novel molecular mechanisms that drive complex molecular pathologies. Further development would allow for refinement of this approach to individual patient targeting both by studying the exact biological mechanism of the *IKZF1* immune-recruitment phenotype, and by extending the analysis to search for recruitment master regulators of other immune cell types. For the analysis specifically of the *IKZF1* aQTL, the potential amenable cohort size across the TCGA ranged from 25% to 60%, indicating significant potential for clinical development and broad application.

We have established the precedent that computational methods such as DIGGIT provide a framework that can contribute to multiple key goals of precision medicine. Adding to the emerging body of work focused specifically on using master regulators to identify actionable targets, we show that these approaches can be leveraged not only to identify master regulators that affect tumor cell-autonomous physiologies, e.g., mesenchymal transformation (Carro et al., 2010), but also to discover novel interaction networks that mediate immune infiltration in cancer. As a corollary, we can identify patient cohorts that may be amenable to specific treatment regimens. Network-based approaches have repeatedly demonstrated their promise in driving the development of precision medicine, and our work highlights the potential of identifying and leveraging master regulators with the goal of enhancing cancer immunotherapy.

STAR★METHODS

Detailed methods are provided in the online version of this paper and include the following:

- KEY RESOURCES TABLE
- CONTACT FOR REAGENT AND RESOURCE SHARING
- EXPERIMENTAL MODELS AND SUBJECT DETAILS
- METHOD DETAILS
  - TCGA Data and Prognostic Quantification
  - ARACNe, DIGGIT Networks and Subsequent Interrogation
  - Infiltration Signatures
  - Cell Culture and Transductions
  - RNAseq Processing and Analysis
  - Mouse Model and Methods
  - Tumor Cell Isolation
  - Flow Cytometry and Antibodies
  - Cytotoxicity Assays
- QUANTIFICATION AND STATISTICAL ANALYSIS
- DATA SOFTWARE AND AVAILABILITY

SUPPLEMENTAL INFORMATION

Supplemental Information includes five figures and six tables and can be found with this article online at https://doi.org/10.1016/j.cels.2018.05.020.

ACKNOWLEDGMENTS

We thank Dr. Charles Karan and the High-Throughput Screening Facility at Columbia University Medical Center for the human cancer cell lines used in this project. We thank Drs. Andrea Califano, Wendy Chung, Ali Gharavi, Ronald Wapner, and Krzysztof Kiryluk for their insightful discussions related to the work. J.C.C. was supported by the Columbia University Herbert and Florence Irving Medical Center Dean's Precision Medicine Research Fellowship (UL1TR001873). These studies utilized the resources of the EpiCURE Skin Disease Research Core Center (P30AR069632) as well as the Flow Cytometry Shared Resource and the Human Immune Monitoring Core of the Herbert Irving Comprehensive Cancer Center (P30CA013696).

AUTHOR CONTRIBUTIONS

The conceptual framework for this project was developed by J.C.C. and A.M.C. J.C.C. implemented and performed the computational analysis and in vitro experiments. R.P.-L. performed the mouse experiments and associated analysis. Y.M.S. provided an independent human melanoma cohort data and assisted with its analysis. C.G.D. provided expertise for immune cell analysis and interpretation of immunotherapy data. The manuscript was written by J.C.C. and A.M.C., and all authors participated in editing of the final manuscript.

DECLARATION OF INTERESTS

The authors declare no competing interests.

Received: January 8, 2018
Revised: March 7, 2018
Accepted: May 25, 2018
Published: June 27, 2018

REFERENCES

Aggen, D.H., and Drake, C.G. (2017). Biomarkers for immunotherapy in bladder cancer: a moving target. J. Immunother. Cancer *5*, 94.

Alvarez, M.J., Chen, J.C., and Califano, A. (2015). DIGGIT: a Bioconductor package to infer genetic variants driving cellular phenotypes. Bioinformatics *31*, 4032–4034.

Ascierto, P.A., Simeone, E., Sznol, M., Fu, Y.-X., and Melero, I. (2010). Clinical experiences with anti-CD137 and anti-PD1 therapeutic antibodies. Semin. Oncol. *37*, 508–516.

Bindea, G., Mlecnik, B., Tosolini, M., Kirilovsky, A., Waldner, M., Obenauf, A.C., Angell, H., Fredriksen, T., Lafontaine, L., Berger, A., et al. (2013). Spatiotemporal dynamics of intratumoral immune cells reveal the immune landscape in human cancer. Immunity *39*, 782–795.

Califano, A. (2014). Predicting protein networks in cancer. Nat. Genet. *46*, 1252–1253.

Carro, M.S., Lim, W.K., Alvarez, M.J., Bollo, R.J., Zhao, X., Snyder, E.Y., Sulman, E.P., Anne, S.L., Doetsch, F., Colman, H., et al. (2010). The transcriptional network for mesenchymal transformation of brain tumours. Nature *463*, 318–325.

Chen, J.C., Alvarez, M.J., Talos, F., Dhruv, H., Rieckhof, G.E., Iyer, A., Diefes, K.L., Aldape, K., Berens, M., Shen, M.M., and Califano, A. (2014). Identification of causal genetic drivers of human disease through systems-level analysis of regulatory networks. Cell *159*, 402–414.

Chen, J.C., Cerise, J.E., Jabbari, A., Clynes, R., and Christiano, A.M. (2015). Master regulators of infiltrate recruitment in autoimmune disease identified through network-based molecular deconvolution. Cell Syst. *1*, 326–337.

Dong, H., Strome, S.E., Salomao, D.R., Tamura, H., Hirano, F., Flies, D.B., Roche, P.C., Lu, J., Zhu, G., Tamada, K., et al. (2002). Tumor-associated B7-H1 promotes T-cell apoptosis: a potential mechanism of immune evasion. Nat. Med. *8*, 793–800.

Drake, C.G., Jaffee, E., and Pardoll, D.M. (2006). Mechanisms of immune evasion by tumors. Adv. Immunol. *90*, 51–81.

Dunn, G.P., Bruce, A.T., Ikeda, H., Old, L.J., and Schreiber, R.D. (2002). Cancer immunoediting: from immunosurveillance to tumor escape. Nat. Immunol. *3*, 991–998.

Emambux, S., Tachon, G., Junca, A., and Tougeron, D. (2018). Results and challenges of immune checkpoint inhibitors in colorectal cancer. Expert Opin. Biol. Ther. *6*, 1–13.

Godfrey, J., Bishop, M.R., Syed, S., Hyjek, E., and Kline, J. (2017). PD-1 blockade induces remissions in relapsed classical Hodgkin lymphoma following allogeneic hematopoietic stem cell transplantation. J. Immunother. Cancer *5*, 11.

Hinz, S., Pagerols-Raluy, L., Oberg, H.-H., Ammerpohl, O., Grüssel, S., Sipos, B., Grützmann, R., Pilarsky, C., Ungefroren, H., Saeger, H.-D., et al. (2007). Foxp3 expression in pancreatic carcinoma cells as a novel mechanism of immune evasion in cancer. Cancer Res. *67*, 8344–8350.

Jabbari, A., Cerise, J.E., Chen, J.C., Mackay-Wiggan, J., Duvic, M., Price, V., Hordinsky, M., Norris, D., Clynes, R., and Christiano, A.M. (2016). Molecular signatures define alopecia areata subtypes and transcriptional biomarkers. EBioMedicine *7*, 240–247.

Kusmartsev, S., and Gabrilovich, D.I. (2006). Role of immature myeloid cells in mechanisms of immune evasion in cancer. Cancer Immunol. Immunother. *55*, 237–245.

Lefebvre, C., Rajbhandari, P., Alvarez, M.J., Bandaru, P., Lim, W.K., Sato, M., Wang, K., Sumazin, P., Kustagi, M., Bisikirska, B.C., et al. (2010). A human B-cell interactome identifies MYB and FOXM1 as master regulators of proliferation in germinal centers. Mol. Syst. Biol. *6*, 377.

Margolin, A.A., Nemenman, I., Basso, K., Wiggins, C., Stolovitzky, G., Dalla-Favera, R., and Califano, A. (2006). ARACNE: an algorithm for the reconstruction of gene regulatory networks in a mammalian cellular context. BMC Bioinformatics *7* (*Suppl 1*), S7.

Min, L., and Hodi, F.S. (2014). Anti-PD1 following ipilimumab for mucosal melanoma: durable tumor response associated with severe hypothyroidism and rhabdomyolysis. Cancer Immunol. Res. *2*, 15–18.

Rizvi, N.A., Mazières, J., Planchard, D., Stinchcombe, T.E., Dy, G.K., Antonia, S.J., Horn, L., Lena, H., Minenza, E., Mennecier, B., et al. (2015). Activity and safety of nivolumab, an anti-PD-1 immune checkpoint inhibitor, for patients with advanced, refractory squamous non-small-cell lung cancer (CheckMate 063): a phase 2, single-arm trial. Lancet Oncol. *16*, 257–265.

Sivendran, S., Chang, R., Pham, L., Phelps, R.G., Harcharik, S.T., Hall, L.D., Bernardo, S.G., Moskalenko, M.M., Sivendran, M., Fu, Y., et al. (2014). Dissection of immune gene networks in primary melanoma tumors critical for antitumor surveillance of patients with stage II-III resectable disease. J. Invest. Dermatol. *134*, 2202–2211.

Subramanian, A., Tamayo, P., Mootha, V.K., Mukherjee, S., Ebert, B.L., Gillette, M.A., Paulovich, A., Pomeroy, S.L., Golub, T.R., Lander, E.S., and Mesirov, J.P. (2005). Gene set enrichment analysis: a knowledge-based approach for interpreting genome-wide expression profiles. Proc. Natl. Acad. Sci. USA *102*, 15545–15550.

Topalian, S.L., Drake, C.G., and Pardoll, D.M. (2015). Immune checkpoint blockade: a common denominator approach to cancer therapy. Cancer cell *27*, 450–461.

Valecha, G.K., Vennepureddy, A., Ibrahim, U., Safa, F., Samra, B., and Atallah, J.P. (2017). Anti-PD-1/PD-L1 antibodies in non-small cell lung cancer: the era of immunotherapy. Expert Rev. Anticancer Ther. *17*, 47–59.

Verhaak, R.G.W., Hoadley, K.A., Purdom, E., Wang, V., Qi, Y., Wilkerson, M.D., Miller, C.R., Ding, L., Golub, T., Mesirov, J.P., et al. (2010). Integrated genomic analysis identifies clinically relevant subtypes of glioblastoma characterized by abnormalities in PDGFRA, IDH1, EGFR, and NF1. Cancer Cell *17*, 98–110.

Woo, J.H., Shimoni, Y., Yang, W.S., Subramaniam, P., Iyer, A., Nicoletti, P., Rodríguez Martínez, M., López, G., Mattioli, M., Realubit, R., et al. (2015). Elucidating compound mechanism of action by network perturbation analysis. Cell *162*, 441–451.

Xing, L., Dai, Z., Jabbari, A., Cerise, J.E., Higgins, C.A., Gong, W., de Jong, A., Harel, S., DeStefano, G.M., Rothman, L., et al. (2014). Alopecia areata is driven by cytotoxic T lymphocytes and is reversed by JAK inhibition. Nat. Med. *20*, 1043–1049.

STAR★METHODS

KEY RESOURCES TABLE

REAGENT or RESOURCE	SOURCE	IDENTIFIER
Antibodies		
Rat IgG2a anti-CD279, clone RMP1-14	Bioxcell	BE0146; RRID: AB_10949053
Mouse IgG2b anti CD152, clone 9D9	Bioxcell	BE0164; RRID: AB_10949609
Rat IgG2a, clone 2A3	Bioxcell	BE0089; RRID: AB_1107769
Mouse IgG2b, clone MPC-11	Bioxcell	BE0086; RRID: AB_1107791
CD19-FITC, eBio1D3	eBioscience	11-0193-82; RRID: AB_657666
NK1.1-PE, PK136	eBioscience	14-5941-81; RRID: AB_467735
Foxp3-APC, FJK-16s	eBioscience	17-5773-82; RRID: AB_469457
Anti-CD11c-PE/Dazzle 594, N418	BioLegend	117347; RRID: AB_2563654
CD45-Brilliant violet 605, 30-F11	BioLegend	103139; RRID: AB_2562341
CD4-Brilliant Violet 510, GK1.5	BioLegend	100449; RRID: AB_2564587
CD8a-Brilliant Violet 711, 53-6.7	BioLegend	100747; RRID: AB_11219594
Bacterial and Virus Strains		
pMD2.G	Addgene	Addgene plasmid # 12259
pCMV8.74	Addgene	Addgene plasmid # 22036
Chemicals, Peptides, and Recombinant Proteins		
pLOC	ThermoFisher / Open Biosystems	OHS5830
Critical Commercial Assays		
Cytotox 96 Non-Radioactive Cytotoxicity Assays	Promega	G1780
Deposited Data		
The Cancer Genome Atlas Cancer cohorts	TCGA	https://tcga-data.nci.nih.gov/docs/publications/tcga/?
RNAseq data, human and mouse	This manuscript	GSE111201
Independent Melanoma cohort expression data	Sivendran et al., 2014	https://doi.org/10.1038/jid.2014.85
Experimental Models: Cell Lines		
SKMEL2	ATCC	HTB-68
NCIH441	ATCC	HTB-174
TCCSUP	ATCC	HTB-5
LNCAP	ATCC	CRL-1740
8505C	JCRB	JCRB0826
SF210	UCSF	SF210
B16F10	Columbia University EPICURE Core	EPICURe-B16F10
CT26	ATCC	CRL-2638
MYCCAP	ATCC	CRL-3255
Experimental Models: Organisms/Strains		
Mouse: Black6	Jackson Labs	https://www.jax.org/strain/000664
Mouse: Nude	Tacomic Farms	NCRNU-F/M
Software and Algorithms		
DIGGIT	Bioconductor	https://www.bioconductor.org/
ARACNe	Bioconductor	https://www.bioconductor.org/
MeV	Sourceforge	https://sourceforge.net/projects/mev-tm4/
FCS Express 6	De Novo Software	https://www.denovosoftware.com/site/Flow-RUO-Overview.shtml
Other		
RNAseq QC and processing	Columbia University Genome Center	https://systemsbiology.columbia.edu/genome-center

CONTACT FOR REAGENT AND RESOURCE SHARING

Further information and requests for resources and reagents should be directed to and will be fulfilled by the Lead Contact, Angela Christiano (amc65@cumc.columbia.edu).

EXPERIMENTAL MODELS AND SUBJECT DETAILS

Seven-week old female C57BL6/J and athymic mice ($NCr^{nu/nu}$) were purchased from The Jackson Laboratory or Taconic Farms respectively. All animals were kept under a controlled environment of temperature and humidity and a 12h light/dark cycle. Experimental procedures were in compliance with a Columbia University Institutional Animal Care and Use Committee approved protocol.

The following human-derived cancer cell lines used in this study were obtained courtesy of the Drug Screening Facility at Columbia University along with relevant documentation (through the ATCC): 8505c (thyroid), LNCaP (prostate), D04 (melanoma), SKCM-MEC2 (melanoma), TCCSUP (bladder), NCIH441 (lung); and SF210 (glioblastoma) from UCSF. Cell lines were cultured, passaged, and maintained in accordance with the guidelines provided in these documents (see Key Resources Table for details). All relevant information on each individual line is detailed in the associated, publicly available documents. Mouse B16F10 lines were made available through Dr. David Owens and the EPICURE Core at Columbia University Medical Center, MyCCap from Dr. Charles Drake, and RENCA and CT26 from the ATCC. B16F10 was cultured with DMEM 10%FBS, MYCCAP and CT26 with RMPI1640 10%FBS, all stored at 37C, 5% CO2.

METHOD DETAILS

TCGA Data and Prognostic Quantification

Level 3 copy number variation data (Agilent CGH arrays) and accompanying RNAseq data were downloaded for each of the following TCGA datasets: SKCM, GBM, HNSC, LUAD/LUSC, THCA, BLCA, PRAD, UCEC, KIRC, COAD, READ, LIHC, LGG, STAD. Accompanying clinical annotations were also downloaded and stored as an R object for reference. These data are all open access via The Cancer Genome Atlas Data Portal (https://gdc.cancer.gov/).

ARACNe, DIGGIT Networks and Subsequent Interrogation

The ARACNe and DIGGIT algorithm are publicly available via Bioconductor, and their application is fully detailed in (Margolin et al., 2006; Lefebvre et al., 2010; Chen et al., 2014; Alvarez et al., 2015). For specific methodology and function of these algorithms please refer to these references.

These algorithms were applied to each of the indicated TCGA datasets to generate all fCNVs and their associated aQTLs for each cancer set. The immune infiltrate recruitment signature was derived from the validation experiments in (Chen et al., 2015), which cross-referenced the AAGS with IKZF1 validated targets (validated via exogenous expression and RNAseq analysis). Each of these regulons was used as the input molecular signature for all DIGGIT networks to generate specific driver candidates and aQTLs. The output of this analysis is an ordered list of candidate aQTLs that can be ranked by p-value of statistical enrichment with the target gene signature. The distribution of each of these signatures was tested against randomized gene panels by the Mann-Whitney U-test using an FDR threshold of 0.05.

For each cancer passing this threshold, the top aQTL clusters were tested for association with prognosis by separating cohorts into two bins: patients with no functional mutations in the tested cluster, or patients with at least one functional mutation in the cluster. These groups were then filtered for patients with a confirmed date of death in the dataset and cross-referenced with the post-diagnostic survival. This allowed the assessment of association with survival using the U-test for median survival, Mantel-Cox for survival progression, and Fisher's Exact for rates of death at alpha 0.05.

For the purposes of calling CNVs in individual patients in genomic analysis, a standard threshold of $|\text{callvalue}|>0.168$ was used on $\log_{10}$ call values, corresponding to a copy number change signal >1.5(Chen et al., 2014). For testing associations to clinical outcomes and immune infiltrates, patient genomic matrices were converted to binary values for CNV calls (1 for positive call, mutation exists; and 0 for evidence of diploid/normal locus). These calls were used to segregate patients into appropriate cohorts for statistical testing. Unless otherwise specified, differential expression and Fisher's Exact Test significance was ascertained using a standard threshold of FDR<0.05.

Infiltration Signatures

Infiltration signatures have been extensively characterized in previous studies and used to estimate relative infiltrate compositions in tissues. Using these signatures (Bindea et al., 2013), as we have done in previous work (Jabbari et al., 2016), we generated quantitative estimators of each infiltrate cell type or category by integrating the overall relative signal of these marker panels in the tumor samples. This was achieved using either averaged z-normalized expressed signatures to compute consensus fold change and fisher integration of p-values of differential expression. Both methods produced concordant results and results were reported as a bivariate measure using both metrics.

Cell Culture and Transductions

The IKZF1 and RFP cassette genes were subcloned for transduction into a modified pLOC expression vector bearing a multiple cloning site. This standard vector is the same backbone that has been used in previous studies. Subcloning was performed and colonies were validated by Sanger sequencing via GeneWiz (https://www.genewiz.com/en).

Transfections were performed using the JetPRIME (http://www.polyplus-transfection.com/products/jetprime/) reagent according to manufacturer protocols, 1:2 DNA:reagent ratio. Transfections were tested in target cell lines and 293T cells (hosts for lentivirus production) and validated by PCR and fluorescence microscopy.

Lentiviral transfections into 293T were done with the pMD2.G and pCMV8.74 (Addgene plasmid #12259, Addgene plasmid #22036) packaging plasmids, scaling to 3ug of target plasmid for a 10cm plate in serum-free media (3mL overnight). The following day and 24 hours after transfection, virus-bearing media was syringe filtered and viral particles were precipitated overnight at 4C using Peg-IT viral precipitating media (https://www.systembio.com/products/lentivirus-production/virus-concentration-and-titering/peg-it-virus-precipitation-solution/). Viral titer was aliquotted and pelleted for dry-pellet storage at −80C or use in experiments.

For transduction, pellets were resuspended in the appropriate media for each cell line and placed over 50-60% confluent cells in six-well format. A total of 1mL of virus-bearing media was used per transduction. Transduction was repeated 24 hours later with fresh viral titer. Following infection, cells were placed on blasticidin selection at 5ug/ml for seven days. After selection, cells were maintained on 1ug/ml blastiticidin. Prior to amplification for grafting, cells were sorted for GFP production (IKZF1) or RFP and GFP production (RFP) to maximize purity.

RNAseq Processing and Analysis

Total RNA samples were isolated from cell populations frozen in TRIzol after experimentation. All samples were isolated and purified simultaneously using RNA prep kits available through Qiagen. RNA concentration and quality was assessed by Bioanalyzer via the core facilities at Columbia University and submitted to the Genome Center at Columbia University for processing. RNAseq results were retrieved from the Center in accordance to their standard QC and analytic pipeline.

Subsequent analyses for differential expression and Gene Set Enrichment Analysis (GSEA) (Subramanian et al., 2005) were conducted using standard analytic packages available in R via Bioconductor. In all circumstances an alpha of 0.05 was used for the threshold defining differential expression to better facilitate network-based analysis (Lefebvre et al., 2010). GSEA (Subramanian et al., 2005; Woo et al., 2015) was conducted using this data and the validated IKZF1 regulon provided in (Chen et al., 2015).

Mouse Model and Methods

Subcutaneous melanomas were generated by *s.c*. Injection of $5x10^4$ B16F10 tumor cells [obtained from Dr. David Owens at the Columbia University Skin Disease Resource-Based Center (epiCURE)], with or without the forced expression of human IKZF-1, into the right the flank of C57BL/6 or NCr nude mice. For the immunotherapy experiments, animals were randomly assigned to different groups and starting on day 5 received three *i.p*. injections (three days apart) of either anti PD1 (Rat IgG2a anti-CD279, clone RMP1-14), anti CTLA4 (Mouse IgG2b anti CD152, clone 9D9) monoclonal antibodies or the corresponding isotype controls (Clones 2A3 and MPC-11 respectively), all from Bioxcell. Tumor size was measured daily with a caliper, and their volumes calculated by using the ellipsoid formula (d^2xD)x0.52, where D represents the greatest diameter and d represents the smallest diameter. Mice were sacrificed when tumor exceeded 20 mm in diameter.

Tumor Cell Isolation

Subcutaneous B16 melanoma tumors were excised from the animals at the end of the experiments. Tumor infiltrating lymphocytes were prepared in a discontinuous Percoll (GE Healthcare) gradient by collecting the interface between the 40 and 80% layers.

Flow Cytometry and Antibodies

The anti-mouse antibodies CD19-FITC (clone eBio1D3), NK1.1-PE (clone PK136), Foxp3-APC (clone FJK-16s) were purchased from eBioscience. Anti-CD11c-PE/Dazzle™ 594 (N418), CD45-Brilliant violet 605™ (30-F11) CD4-Brilliant Violet 510™ (GK1.5), and CD8a-Brilliant Violet 711™ (53-6.7) were from BioLegend. Intracellular staining for Foxp3 was performed using the Foxp3-Transcription factor staining buffer set (eBiosicience) following the manufacturer's protocol. Cells were acquired on a Fortessa flow cytometer (BD Biosciences) and data were analyzed using FCS Express 6 flow software (DeNovo software).

Cytotoxicity Assays

Whole blood PBMCs were isolated using Histopaque (https://www.sigmaaldrich.com/catalog/product/sigma/10771?lang=en&region=US) precipitation using blood provided by healthy donors via the clinic at Columbia University. Isolation was performed the day before cytotoxicity experiments to ensure viability. Transduced target cell lines were cultured as described above in 10cm plates.

Cytotoxicity was assayed using the Cytotox96 kit available from Promega (https://www.google.com/search?q=cytotox&oq=cytotox&aqs=chrome..69i57j0l2j69i65l2j69i61.1103j0j4&sourceid=chrome&ie=UTF-8), as has been done in previous work. The target:PBMC ratio was set to 1:100 and performed in technical quadruplicates in a 96-well plate. Standard manufacturer protocol was followed otherwise.

QUANTIFICATION AND STATISTICAL ANALYSIS

Unless otherwise specified for specific methods (which will be detailed in their respective publications), a statistical threshold of $p<0.05$ corrected for multiple hypothesis testing (False Discovery Rate or Bonferroni correction as indicated) was used. All figures report mean and SEM as the error bars except the box-and-whisker plots which report median, IQR, and $5^{th}/95^{th}$ percentiles. All relevant numbers are disclosed in the corresponding figure legends and sections. Mann-Whitney U-test was used to identify whole shifts in aQTL distribution. All categorical comparisons were done by Fisher's Exact Test. Statistical significance in survival was determined using KM survival curves and associated statistics. Differences in cytotoxic sensitivity were assayed by T-test. Gene Set Enrichment Analysis was conducted using bootstrapped, shuffled data to generate random distributions (10k iterations), which were used to compute the normalized enrichment score as detailed in previously published literature. For flow quantification and CD4+ CD8+ ratios, the paired T-test was used. For tumor growth, two-way ANOVA with Bonferroni's post-test was used to determine significant differences between treatment groups.

DATA SOFTWARE AND AVAILABILITY

All RNA-seq data generated specifically in this study are publicly available at the Gene Expression Omnibus under accession number GEO: GSE111201. All TCGA data used are available through their respective data portal. Independent melanoma cohorts used in this study are available as supplemental materials via Sivendran et al. (2014). All algorithms used in this study are publicly available through Bioconductor R packages.